Flat bands and gaps in twisted double trilayer graphene

F. J. Culchac [1,2,*] R. R. Del Grande [1,3] Marcos G. Menezes [1] and Rodrigo B. Capaz [1,4]

[1]*Instituto de Física, Universidade Federal do Rio de Janeiro, Rio de Janeiro, RJ 21941-972, Brazil*

[2]*Departamento de Física, Universidad del Valle, Cali, Colombia*

[3]*Department of Physics, University of California, Merced, California 95343, USA*

[4]*Brazilian Nanotechnology National Laboratory (LNNano), Brazilian Center for Research in Energy and Materials (CNPEM), 13083100, Campinas, SP, Brazil*

(Received 12 December 2024; revised 20 January 2025; accepted 22 January 2025; published 5 February 2025)

We study the electronic band structure of twisted double trilayer graphene. This system consists of two regularly stacked graphene trilayers rotated by a given angle. We consider two different arrangements for the trilayer units following their stackings: ABA-ABA and ABC-ABC. First-principles calculations at an angle of 13.1° show that these two systems are semiconductors with narrow gaps, which result from a reduced symmetry due to the presence of the second trilayer. Next, we use these results to build a tight-binding model to study lower twist angles, which are not accessible to first-principles methods. In both cases, we find that, as the angle decreases, the magnitude of the gap decreases and eventually closes. At the same time, the low-energy bands develop into flat bands. The corresponding magic angle is greater than the values found in twisted bilayer graphene and twisted double bilayer graphene, thus supporting a hypothesis that it should increase as a function of the number of stacked layers in the rotating unit. We also discuss the spatial separation of the electronic states and their hybrization as a function of the twist angle, as well as the behavior of the systems under an external electric field. We find patterns that are reminiscent of the behaviors found in gated ABA and ABC trilayers, such as tunable overlaps or band gaps, respectively.

DOI: 10.1103/PhysRevB.111.075111

I. INTRODUCTION

In two-dimensional (2D) materials, the twist angle between stacked layers leads to symmetry breaking and strain effects, allowing enhanced or suppressed interlayer coupling [1–4]. In twisted bilayer graphene (TBG), when the twist angle is small, there is an interlayer hybridization that leads to the emergence of flat bands with narrow bandwidth. This twist angle is called "magic angle." The flat bands and strong many-body effects lead to correlated insulating states and superconductivity [5–7], ferromagnetism [8–10], and magnetic-field-induced Chern insulators [11–13]. The studies of TBG were extended to other graphene superlattices which showed extraordinary physical properties near the flat electronic band, such as twisted mono-bilayer graphene [14,15] and twisted double bilayer graphene (TDBG) [16–21]. Experimental works reported supercondutivity [22,23] for twisted trilayer graphene (TTG), which consists of three adjacent graphene layers sequentially twisted by θ and $-\theta$. This system has a magic angle $\theta \approx 1.6^{o}$, a value that is slightly higher than the magic angle for TBG and TDBG. Additionally, optical properties in twisted multilayer graphene structures were studied as a function of the twist angle. It was predicted that the value of the magic angle should increase with the number of stacked layers [24]. More recently, twisted double trilayer graphene (TDTG) systems have been investigated. In the case of ABC-TDTG, a theoretical work showed that for a small twist angle there is a charge redistribution within the layers [25] and an experimental work showed electric transport measurements for small angles [26]. In this article, we perform a systematic study of the evolution of the energy gap, the flat bands and the effect of the electric field in ABC-TDTG and ABA-TDTG systems as a function of the rotation angle. We also study the degree of localization of the electronic states in the different layers of the systems.

In this work, we employ a combination of first-principles calculations and the tight-binding formalism to study two different types of Moiré graphene multilayer systems based on TDTG. The first case consists of two ABC-stacked trilayers with a rotation between them (ABC-TDTG). When only one ABC trilayer is considered, the low-energy bands consist of a pair of bands with cubic dispersion, which are very flat near the Fermi level [27–29]. As we shall see, in ABC-TDTG the cubic dispersion persists but now there is an energy gap that depends on the twist angle. Another system studied is composed of two ABA-stacked trilayers with a rotation between them (ABA-TDTG). For a single ABA trilayer, the bands consist of a set of monolayer and bilayer-like bands, with linear and quadratic dispersions, respectively [30–32]. When another ABA trilayer is added and rotated, the system shows a gap and an anticrossing between energy bands near the Fermi energy. For both systems, we observe flat bands for small twist angles, so they provide a platform for investigating the properties of a semiconducting flat band Moiré–van der Waals heterostruture.

*Contact author: culchac@if.ufrj.br

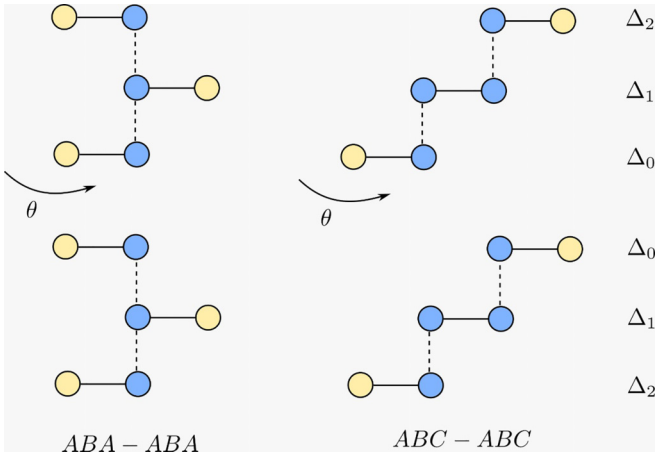

FIG. 1. Schematic representation of twisted double trilayer graphene for two ABC-stacked trilayers (left) and two ABA-stacked trilayers (right). Δ_o, Δ_1, and Δ_2 are the on-site terms of inner, middle and outer layers, respectively. Blue-colored spheres indicate carbon atoms that are on top of each other in each trilayer, while yellow-colored spheres indicate atoms that lie on top of hexagon centers.

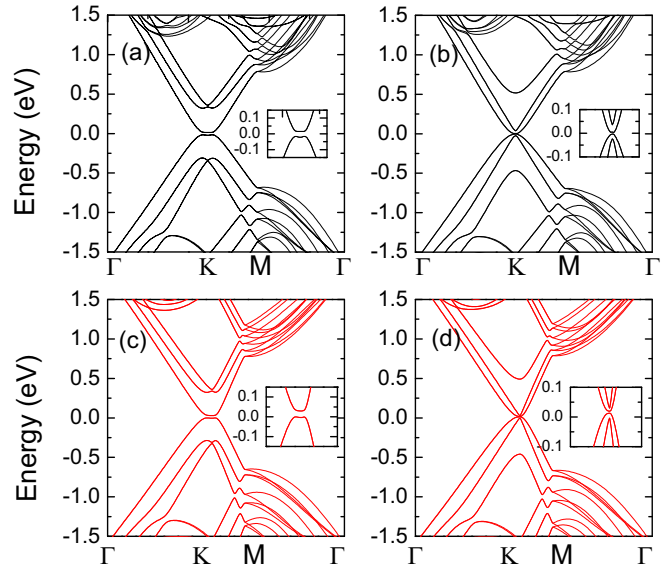

FIG. 2. Band structures calculated with QE for two systems (a) ABC-TDTG and (b) ABA-TDTG for a twist angle $\theta = 13.1^{\circ}$. For comparison, we show the band structures calculated with a full TB model for the (c) ABC-TDTG and (d) ABA-TDTG. We approximately reproduce the DFT gaps in both cases by using the on-site energies $\Delta_0 = 0$, $\Delta_1 = 20\,\text{meV}$, and $\Delta_2 = 30\,\text{meV}$ (see text). The insets show a zoom near the K point.

II. THEORY

A. Unit cell

TDTGs are composed of six graphene layers with one twist parameter θ. Figure 1 shows ABC- and ABA-stacked trilayers rotated by an angle θ. For graphene multilayer systems, it was shown that the electrostatic potential of the layers can be different due to different chemical environments between inner and outer layers [20]. These potentials can be controlled by a parameter Δ in a tight- binding model. For this reason, we define Δ_0, Δ_1 and Δ_2 as the on-site energies of inner, middle and outer layers, respectively.

It is also important to mention that single ABA and ABC trilayers have different symmetries. In particular, while ABA has a mirror plane containing the middle layer, ABC has inversion symmetry. This difference leads to the observed low-energy dispersions mentioned in the introduction and to different behaviors under the influence of an external electric field, which can be modeled as a nonzero value of the difference $\Delta_2 - \Delta_0$ [25]. The presence of an additional trilayer is expected to introduce similar effects, by modifying the chemical environment of the layers through mechanisms such as charge transfer. Therefore, all three energies are considered as independent parameters, which are adjusted to reproduce our DFT calculations for large twist angles.

B. DFT calculations

Our DFT calculations were performed with the Quantum Espresso code [33,34]. The wave functions were expanded in a plane wave basis with an energy cutoff of 80.0 Ry. We have used norm-conserving pseudopotentials for the electron-ion interaction and a vdw-df-obk8 exchange-correlation functional, which includes van der Waals interactions [35]. Recent calculations revealed that this functional provides an optimal overall description of the structural and vibrational properties of multilayer graphene and graphite [36], so it is an ideal choice for the present case. We have chosen the two smallest supercells, $\theta = 21.8^{\circ}$ and $\theta = 13.1^{\circ}$, as *ab initio* calculations in larger cells become prohibitive. Both ABA and ABC stackings within each trilayer were considered. The Brillouin zones of the $\theta = 21.8^{\circ}$ (13.1°) supercells were sampled in a $4 \times 4 \times 1$ ($3 \times 3 \times 1$) Monkhorst-Pack k-point grid [37]. In addition, we have included a vacuum of 20 Å in the (Z) direction, perpendicular to the layers. The atomic positions were relaxed until all forces were smaller than 10^{-3} Ry/bohr and the total energies changed by less than 10^{-4} Ry. The primitive vectors of the supercell in the XY plane were also relaxed to a target pressure of zero with a tolerance of 0.5 kbar.

C. Tight-binding model

The full TB Hamiltonian employed in the article, including the on-site energies, is an extension of a previous model [38]

$$H = \sum_i \Delta_i \, |i\rangle \, \langle i| - \sum_{i \neq j} t(\mathbf{R}_i - \mathbf{R}_j) \, |i\rangle \, \langle j| \, ,$$

where $\Delta_0 = 0$, $\Delta_1 = 20\,\text{meV}$, and $\Delta_2 = 30\,\text{meV}$ are the on-site energy of sites in inner, middle, and outer layers, respectively. We use the same energies for the ABA-TDTG and ABC-TDTG systems, as the resulting TB band structures are found to reproduce the main features observed in our DFT calculations for large twist angles, as we show below (see Fig. 2). The distance-dependent hopping parameter $t(\mathbf{d})$ is

given by

$$-t(\mathbf{d}) = V_{pp\pi}(d)\left[1-\left(\frac{\mathbf{d}\cdot\mathbf{e_z}}{d}\right)^2\right] + V_{pp\sigma}(d)\left(\frac{\mathbf{d}\cdot\mathbf{e}_z}{d}\right)^2,$$

$$V_{pp\pi}(d) = V^0_{pp\pi}\exp\left(-\frac{d-a_0}{r_0}\right),$$

$$V_{pp\sigma}(d) = V^0_{pp\sigma}\exp\left(-\frac{d-d_0}{r_0}\right),$$

where $\mathbf{d} = \mathbf{R}_i - \mathbf{R}_j$ is the distance between two atoms, e_z is the unit vector on the z axis. $V^0_{pp\pi} = -2.7$ eV is the intralayer nearest-neighbor hopping in graphene, $a_0 = a/\sqrt{3} = 0.142$ nm is the nearest-neighbor C-C distance in single-layer graphene, $V^0_{pp\sigma} = 0.48$ eV is the interlayer nearest-neighbor hopping and $d_0 = 0.335$ nm is the distance between consecutive layers. The decay length parameter r_0 is chosen to be $0.184a$ to set the value of the intralayer second nearest-neighbor hopping to $0.1V^0_{pp\pi}$.

The effects of atomic relaxations on the electronic structure have also been explored in our TB calculations. Energy minimizations were performed with the LAMMPS [39] package using the Kolmogorov-Crespi potential [40,41] with a cutoff of 20 Å for nonbonded interlayer interactions and the REBO potential [42,43] for bonded intralayer interactions. During minimizations, supercell dimensions (parallel to graphene sheets) were allowed to relax and iterations stop when the sum of absolute values of force components over the entire system is smaller than 0.5 eV/Å.

III. RESULTS AND DISCUSSION

A. ABC-TDTG

The DFT band structures obtained using QE for ABC-TDTG and ABA-TDTG are shown in the Figs. 2(a) and 2(b), respectively. In contrast to the isolated trilayers (in the absence of external fields), these two systems show small gaps energy near the K point. For the ABC-TDTG, the value of the gap is around 32 mev for $\theta = 21.8^o$ and 22 meV for $\theta = 13.1^o$ [Fig. 2(a)]. For ABA-TDTG the gaps between parabolic bands, for $\theta = 21.8^o$ and $\theta = 13.1^o$ [Fig. 2(b)], have the same values, 6 meV. For comparison, the band structures for ABC-TDTG and ABA-TDTG calculated with the TB Hamiltonian for the same twist angle $\theta = 13.1^o$ are shown in Figs. 2(c) and 2(d), respectively. To obtain an excellent agreement with our DFT results, we include in the TB Hamiltonian the on-site energies $\Delta_o = 0$, $\Delta_1 = 20$ meV, and $\Delta_2 = 30$ meV, as defined in Sec. II C.

As we have mentioned above, these energies result from an inequivalence between the inner, middle and outer layers in each trilayer. In fact, the inequivalence between inner and outer layers is already present in isolated layers as a result of their different chemical environments [16,17], but here an additional inequivalence between inner and outer layers is induced by the presence of the second trilayer, in a similar fashion to the observed behavior in TDBG [17].

After obtaining all parameters in our TB model, we proceed to analyze the band structures at small twist angles, which are inaccessible to DFT calculations. The band structures for two small angles in ABC-TDTG are shown in Figs. 3(a) and 3(b). Figure 3(a) shows that for $\theta = 2.65^o$ the band structure has an energy gap Δ_{gap} near the K point. When the twist angle decreases, we begin to observe interesting features as exemplified for the angle 1.61^o [Fig 3(b)]. We observe that the band gap Δ_{gap} closes and new small gaps are opened right above (below) the conduction (valence) bands, as represented by Δ_e and Δ_h in Fig. 3(b). We also observe that the bands become quite flat near the Fermi energy with bandwidths E_w of about 10 meV [5,7].

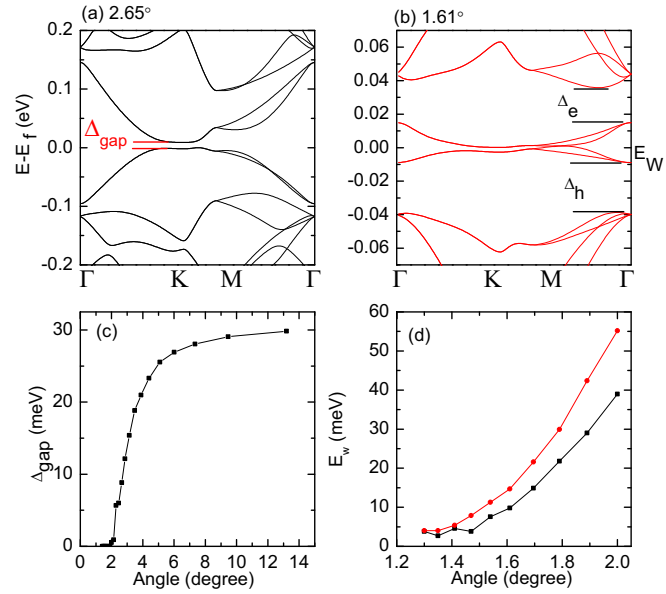

FIG. 3. (a, b) TB band structures calculated for two different twist angles for ABC-TDTG. (c) The value of the gap as a function of the twist angle. (d) Bandwidths E_w of the valence (black dots/line) and conduction (red dots/line) bands as a function of the twist angle.

Figure 3(c) shows that Δ_{gap} decreases when the twist angle decreases and closes for $\theta < 2^o$. The behavior of the bandwidths of the valence and conduction bands can be observed in Fig. 3(d). Considering that E_w becomes smaller than 10 meV for $\theta < 1.61^o$, we can consider this angle as a magic angle for this structure.

B. ABA-TDTG

The band structures for the ABA-TDTG consist in linear Dirac and quadratic dispersion bands. In Figs. 4(a)–4(d) we can observe that the quadratic bands are more sensitive than the linear bands to the variation of the rotation angle. The main characteristics of these quadratic bands are: the energy gap closes, there is an anticrossing between the valence and conduction bands [Fig. 4(b)], and they become flat for small angles. However, the linear bands become relevant for angles close to the magic angle where there is an anticrossing with the quadratic valence band [Fig. 4(d)]. A similar behavior was explained for the case of ABA-stacked trilayer graphene with a gate field perpendicular to the layers [30]. In that case, they showed that a rehybridization of the linear and parabolic low-energy bands is induced due to the breaking of mirror reflection symmetry in the presence of the field. In our case, this symmetry breaking is due to the presence of the second trilayer.

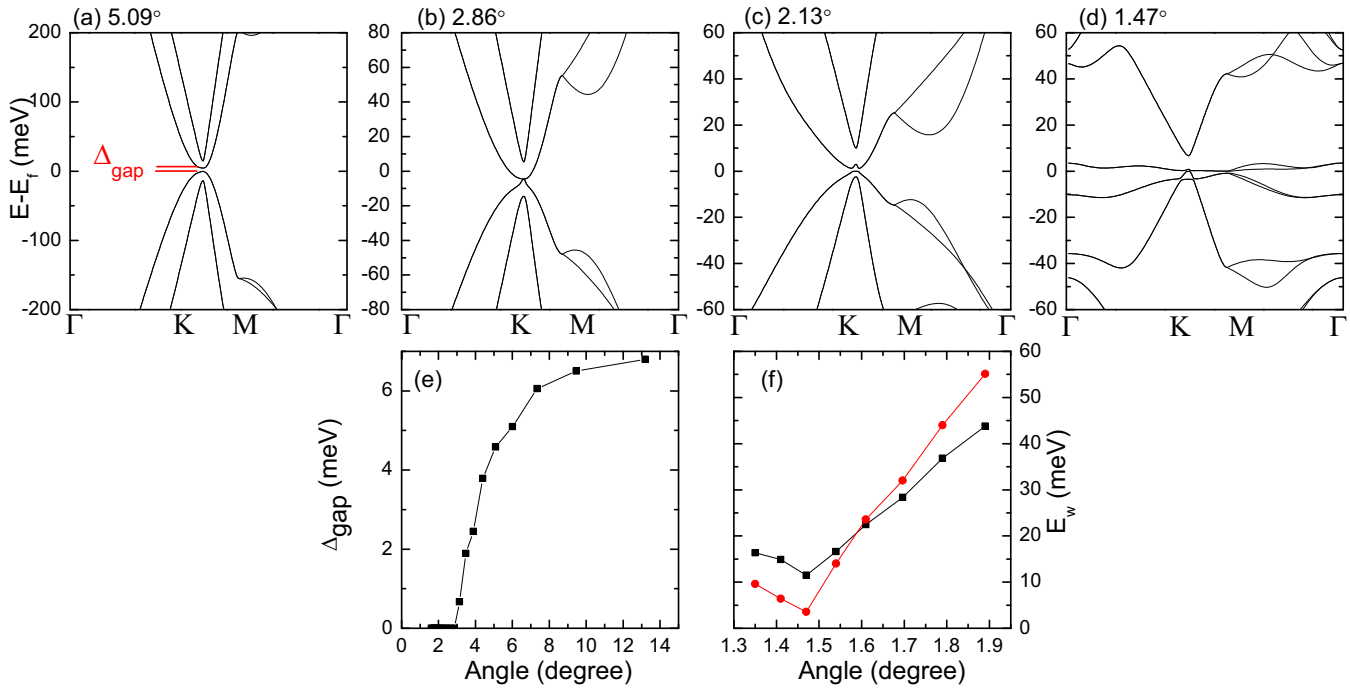

FIG. 4. (a–d) TB band structures for different twist angles for ABA-TDTG. (e) The gap energy as a function of the twist angle. (f) Bandwidths E_w of the valence (black dots/line) and conduction (red dots/line) bands as a function of the twist angle.

The behavior of the energy gap is very similar to the case of ABC-TDTG and TDBG. The size of the energy gap decreases with the rotation angle and closes as it approaches the magic angle. In the case of ABA-TDTG, because it has a smaller energy gap, 6 meV for 13.1°, it will close at a greater angle than the cases mentioned above. The gap closes around 2.86° [Fig. 4(b)]. The bandwidths of the valence and conduction bands as a function of the twist angle is shown in Fig. 4(f). Here, we observe that the bandwidths become smaller than or close to 10 meV for $\theta = 1.47°$, which may be regarded as a magic angle for this structure. Note, however, that the bandwidths increase again for smaller angles, in contrast to ABC-TDTG. This may be due to anticrossing between the quadratic and linear valence bands.

In the case of TBG (two layers), the flat bands were observed for θ around 1.1° [5–7], while in TDBG (four layers) they were seen for a slightly larger angle of around 1.3° [16–21]. Our calculations reveal that in TDTG (six layers) the flat bands arise for a greater angle of approximately 1.6° in ABC-TDTG and 1.47° in ABA-TDTG. With this, we have more evidence for the hypothesis that, by increasing the number of regularly layers with a rotation angle, the magic angle would also increase [24].

Finally, for the ABC-TDTG and ABA-TDTG, we have tested different values of the on-site energies, by varying Δ_1 between 5 and 20 meV and Δ_2 between 10 and 30 meV. In all tests, the systems showed a similar qualitative behavior for the energy gaps and flat bands for small angles, which confirms the robustness of these results.

C. Spatial distribution of electronic states

The spatial distributions of electronic states near the K point for the ABC-TDTG and ABA-TDTG structures are shown in Figs. 5 and 6, respectively. The calculation of the

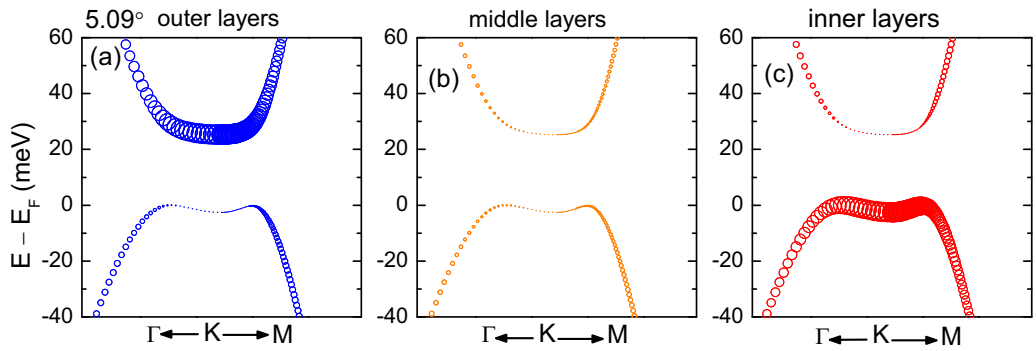

FIG. 5. (a–c) Band structure near the K point for 5.09° for ABC-TDTG. The sizes of blue, orange, and red dots indicate the degree of localization in the inner, middle, and outer layers, respectively.

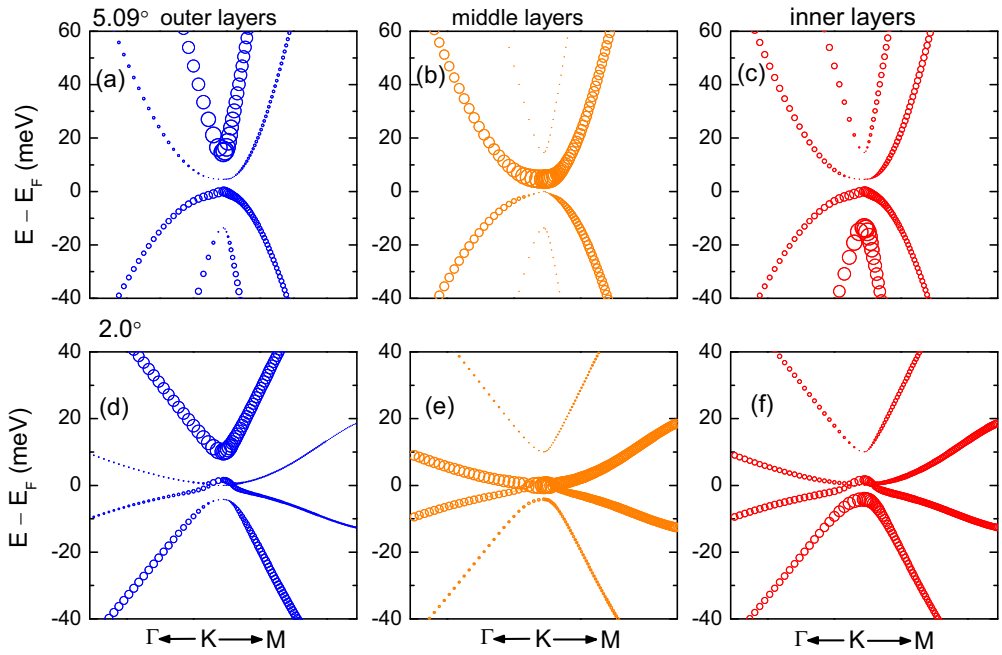

FIG. 6. Band structure near the K point for 5.09° (a–c) and 2.0° (d–f) for ABA-TDTG. The sizes of blue, orange and red dots indicate the degree of localization in the inner, middle, and outer layers, respectively.

spatial distribution for rotated graphene systems was obtained in previous works [17,38]. For both systems, the amount of localization is indicated by the blue, orange and red dots for the outer, middle and inner layers, respectively. In the case of ABC-TDTG with an angle 5.09°, it is possible to observe that the valence (conduction) band is mainly composed of atomic orbitals in the inner (outer) layers, while the contributions from orbitals in the other layers is very low. This behavior has been seen in TDBG [17] where the valence band states display strongly localized states due to AA regions of the inner layers. In addition to this, the electronic localization in ABC-TDTG systems was recently studied in detail [25]. It was observed that, for small angles, there is a charge redistribution within the layers due to Coulomb repulsion in the AA regions between the rotated layers.

For the ABA-TDTG system with 5.09° [Figs. 6(a)–6(c)], it can be seen that the linear conduction (valence) bands are formed mainly by orbitals of the outer (inner) layers, while the quadratic conduction band has a stronger contribution coming from the middle layer and the quadractic valence band has equal contributions from inner and outer layers near the K point. However, for the angle 2.0° [Figs. 6(d)–6(f)], around the magic angle, there is a hybridization between the quadratic and linear bands, as discussed above. As a result, the contributions change. The quadratic bands now present more similar localization patterns, with stronger contributions coming from the middle and inner layers, while the linear bands gain small contributions from the middle layer. This behavior is consistent with an isolated ABA trilayer subjected to an external perpendicular electric field, as explained previously. It also interesting to note that for both ABA and ABC-TDTG, the unequal contributions coming from the outer and inner layers result from a breaking of mirror or inversion symmetry in a trilayer, respectively, due to the presence of the second trilayer.

It is well known that in the case of TBG the Fermi velocity of the linear bands decreases with decreasing angle until these bands become flat [38,44,45]. This same behavior was also observed in AB-twisted trilayer graphene, systems with two layers stacked AB and a third layer rotated with respect to the Bernal staking [46]. Although we did not explicitly calculate the Fermi velocity, it is possible to observe that, in ABA-TDTG (Figs. 4 and 6), the slope of the linear bands decreases with decreasing angle (the horizontal scales are the same in each figure). In this way, these bands have a similar behavior to the two cases mentioned above, the only difference being that for angles close to the magic angle this band does not become flat.

D. Electric field

Finally, we study the effect of an external perpendicular electric field in the electronic structure of the TDTG systems. We find that the band structures for the ABC-TDTG [Figs. 7(a)–7(c)] and ABA-TDTG [Figs. 7(d)–7(f)] display a very similar behavior to the TDBG. The bands, initially degenerate without electric field, are split when the electric field is applied. In the case of ABC-TDTG, the bands near the Fermi level are divided into two groups separated by an energy gap and the flat bands are conserved for small electric field magnitudes [Fig. 7(d)]. The gap size increases with field strength, in a similar fashion to a gated ABC trilayer [28].

For the ABA-TDTG, the degenerate linear bands split into two sets of bands and they hybridize with the flat bands near the Fermi level [Fig. 7(e)]. As the field intensity increases, the hybridization strength increases and the bandwidth of the

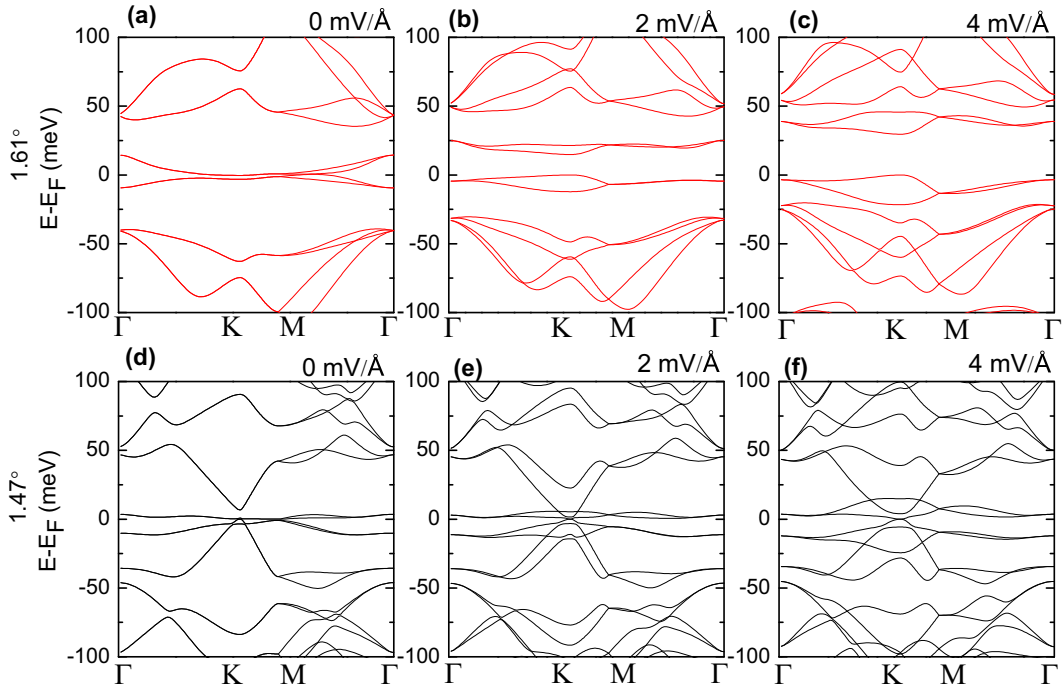

FIG. 7. TB band structures for two twist angles for ABC-TDTG (a–c) and ABA-TDTG (d–f) at various values of electric field.

flat bands increase, while the band gap remains closed. This behavior is consistent with the well-known tunable overlap behavior found in a gated ABA trilayer [30].

IV. CONCLUSIONS

In summary, we study two types of TDTG structures for different rotation angles. These two systems present an energy gap due to the breaking of inversion or mirror symmetry due to presence of the second trilayer. For both ABA and ABC stackings of the rotated trilayers, we see that the band gap of the system decreases and flat bands develop as the rotation angle decreases and approaches the magic angle. We find that this angle is larger than the values found in TBG and TDBG, which is and indication of a general trend that the magic angle should increase as the number of stacked layer in each rotated unit is increased.

In the case of ABA-TDTG, we found that, by changing the rotation angle, it is possible to tune the hybridization of the low-energy bands, in a similar fashion to the behavior found when an external electric field is applied in an isolated ABA trilayer. We also find that the bands with quadratic dispersion are more sensitive to the rotation than the linear bands, as only the former set develop into flat bands for the angles studied. Similarly, for ABC-TDTG, the bands with cubic dispersion develop into flat bands.

Finally, when the multilayer system is subjected to an external electric field perpendicular to the layers, we find that the low-energy bands split into two sets of bands, giving rising to a tunable overlap in ABA-TDTG and a tunable gap in ABC-TDTG. Both trends are consistent with the behavior found in the corresponding isolated trilayer. Additionally, the bandwidth of the flat bands increase with field strength, but they remain flat for magnitudes up to 4mV/Å.

ACKNOWLEDGMENTS

The authors are grateful to the Brazilian funding agencies Coordenação de aperfeiçoamento de pessoal de nível superior (CAPES), Conselho Nacional de Desenvolvimento Científico e Tecnológico (CNPq), Fundação de Amparo à Pesquisa do Estado do Rio de Janeiro (FAPERJ), and Instituto Nacional de Ciência e Tecnologia (INCT)-Nanomateriais de Carbono for financial support and to the High Performance Computing Center (NACAD), COPPE, UFRJ for the use of supercomputing facilities.

DATA AVAILABILITY

No data were created or analyzed in this study.

[1] F. Gargiulo and O. V. Yazyev, Structural and electronic transformation in low-angle twisted bilayer graphene, 2D Mater. **5**, 015019 (2017).

[2] Y.-H. Zhang, D. Mao, Y. Cao, P. Jarillo-Herrero, and T. Senthil, Nearly flat Chern bands in moiré superlattices, Phys. Rev. B **99**, 075127 (2019).

[3] S. Carr, D. Massatt, S. Fang, P. Cazeaux, M. Luskin, and E. Kaxiras, Twistronics: Manipulating the electronic properties of two-dimensional layered structures through their twist angle, Phys. Rev. B **95**, 075420 (2017).

[4] F. Wu, T. Lovorn, E. Tutuc, I. Martin, and A. H. Macdonald, Topological insulators in twisted transition metal

dichalcogenide homobilayers, Phys. Rev. Lett. **122**, 086402 (2019).

[5] Y. Cao, V. Fatemi, A. Demir, S. Fang, S. L. Tomarken, J. Y. Luo, J. D. Sanchez-Yamagishi, K. Watanabe, T. Taniguchi, E. Kaxiras, R. C. Ashoori, and P. Jarillo-Herrero, Correlated insulator behaviour at half-filling in magic-angle graphene superlattices, Nature (London) **556**, 80 (2018).

[6] Y. Cao, V. Fatemi, S. Fang, K. Watanabe, T. Taniguchi, E. Kaxiras, and P. Jarillo-Herrero, Unconventional superconductivity in magic-angle graphene superlattices, Nature (London) **556**, 43 (2018).

[7] M. Yankowitz, S. Chen, H. Polshyn, Y. Zhang, K. Watanabe, T. Taniguchi, D. Graf, A. F. Young, and C. R. Dean, Tuning superconductivity in twisted bilayer graphene, Science **363**, 1059 (2019).

[8] A. L. Sharpe, E. J. Fox, A. W. Barnard, J. Finney, K. Watanabe, T. Taniguchi, M. A. Kastner, and D. Goldhaber-Gordon, Emergent ferromagnetism near three-quarters filling in twisted bilayer graphene, Science **365**, 605 (2019).

[9] X. Lu, P. Stepanov, W. Yang, M. Xie, M. A. Aamir, I. Das, C. Urgell, K. Watanabe, T. Taniguchi, G. Zhang *et al.*, Superconductors, orbital magnets and correlated states in magic-angle bilayer graphene, Nature (London) **574**, 653 (2019).

[10] M. Serlin, C. L. Tschirhart, H. Polshyn, Y. Zhang, J. Zhu, K. Watanabe, T. Taniguchi, L. Balents, and A. F. Young, Intrinsic quantized anomalous Hall effect in a Moiré heterostructure, Science **367**, 900 (2020).

[11] S. Wu, Z. Zhang, K. Watanabe, T. Taniguchi, and E. Y. Andrei, Chern insulators, van Hove singularities and topological flat bands in magic-angle twisted bilayer graphene, Nat. Mater. **20**, 488 (2021).

[12] K. P. Nuckolls, M. Oh, D. Wong, B. Lian, K. Watanabe, T. Taniguchi, B. A. Bernevig, and A. Yazdani, Strongly correlated Chern insulators in magic-angle twisted bilayer graphene, Nature (London) **588**, 610 (2020).

[13] Y. Saito, J. Ge, L. Rademaker, K. Watanabe, T. Taniguchi, D. A. Abanin, and A. F. Young, Hofstadter subband ferromagnetism and symmetry-broken Chern insulators in twisted bilayer graphene, Nat. Phys. **17**, 478 (2021).

[14] H. Polshyn, J. Zhu, M. A. Kumar, Y. Zhang, F. Yang, C. L. Tschirhart, M. Serlin, K. Watanabe, T. Taniguchi, A. H. MacDonald *et al.*, Electrical switching of magnetic order in an orbital Chern insulator, Nature (London) **588**, 66 (2020).

[15] L. Rademaker, I. V. Protopopov, and D. A. Abanin, Topological flat bands and correlated states in twisted monolayer-bilayer graphene, Phys. Rev. Res. **2**, 033150 (2020).

[16] F. Haddadi, Q. S. Wu, A. J. Kruchkov, and O. V. Yazyev, Moiré flat bands in twisted double bilayer graphene, Nano Lett. **20**, 2410 (2020).

[17] F. J. Culchac, R. R. Del Grande, R. B. Capaz, L. Chico, and E. S. Morell, Flat bands and gaps in twisted double bilayer graphene, Nanoscale **12**, 5014 (2020).

[18] G. W. Burg, J. Zhu, T. Taniguchi, K. Watanabe, A. H. MacDonald, and E. Tutuc, Correlated insulating states in twisted double bilayer graphene, Phys. Rev. Lett. **123**, 197702 (2019).

[19] N. R. Chebrolu, B. L. Chittari, and J. Jung, Flat bands in twisted double bilayer graphene, Phys. Rev. B **99**, 235417 (2019).

[20] P. Rickhaus, G. Zheng, J. L. Lado, Y. Lee, A. Kurzmann, M. Eich, R. Pisoni, C. Tong, R. Garreis, C. Gold *et al.*, Gap opening in twisted double bilayer graphene by crystal fields, Nano Lett. **19**, 8821 (2019).

[21] C. Shen, Y. Chu, Q. S. Wu, N. Li, S. Wang, Y. Zhao, J. Tang, J. Liu, J. Tian, K. Watanabe *et al.*, Correlated states in twisted double bilayer graphene, Nat. Phys. **16**, 520 (2020).

[22] J. M. Park, Y. Cao, K. Watanabe, T. Taniguchi, and P. Jarillo-Herrero, Tunable strongly coupled superconductivity in magic-angle twisted trilayer graphene, Nature (London) **590**, 249 (2021).

[23] Z. Hao, A. M. Zimmerman, P. Ledwith, E. Khalaf, D. H. Najafabadi, K. Watanabe, T. Taniguchi, A. Vishwanath, and P. Kim, Electric field–tunable superconductivity in alternating-twist magic-angle trilayer graphene, Science **371**, 1133 (2021).

[24] A. Vela, M. V. O. Moutinho, F. J. Culchac, P. Venezuela, and R. B. Capaz, Electronic structure and optical properties of twisted multilayer graphene, Phys. Rev. B **98**, 155135 (2018).

[25] F. P. Riffo, S. Vizcaya, E. Menéndez-Proupin, J. M. Florez, L. Chico, and E. S. Morell, Behavior of localized states in double twisted ABC trilayer graphene, Carbon **222**, 118952 (2024).

[26] M. L. Perrin, A. Jayaraj, B. Ghawri, K. Watanabe, T. Taniguchi, D. Passerone, M. Calame, and J. Zhang, Electric field tunable bandgap in twisted double trilayer graphene, npj 2D Materials and Applications **8**, 14 (2024).

[27] M. Koshino, Interlayer screening effect in graphene multilayers with *ABA* and *ABC* stacking, Phys. Rev. B **81**, 125304 (2010).

[28] F. Zhang, B. Sahu, H. Min, and A. H. MacDonald, Band structure of *ABC*-stacked graphene trilayers, Phys. Rev. B **82**, 035409 (2010).

[29] L. Zhang, Y. Zhang, J. Camacho, M. Khodas, and I. Zaliznyak, The experimental observation of quantum Hall effect of $l = 3$ chiral quasiparticles in trilayer graphene, Nat. Phys. **7**, 953 (2011).

[30] M. Koshino and E. McCann, Gate-induced interlayer asymmetry in ABA-stacked trilayer graphene, Phys. Rev. B **79**, 125443 (2009).

[31] E. A. Henriksen, D. Nandi, and J. P. Eisenstein, Quantum Hall effect and semimetallic behavior of dual-gated ABA-stacked trilayer graphene, Phys. Rev. X **2**, 011004 (2012).

[32] M. G. Menezes, R. B. Capaz, and S. G. Louie, *Ab initio* quasiparticle band structure of ABA and ABC-stacked graphene trilayers, Phys. Rev. B **89**, 035431 (2014).

[33] P. Giannozzi, S. Baroni, N. Bonini, M. Calandra, R. Car, C. Cavazzoni, D. Ceresoli, G. L. Chiarotti, M. Cococcioni, I. Dabo *et al.*, Quantum espresso: A modular and open-source software project for quantum simulations of materials, J. Phys.: Condens. Matter **21**, 395502 (19pp) (2009).

[34] P. Giannozzi, O. Andreussi, T. Brumme, O. Bunau, M. B. Nardelli, M. Calandra, R. Car, C. Cavazzoni, D. Ceresoli, M. Cococcioni *et al.*, Advanced capabilities for materials modelling with quantum espresso, J. Phys.: Condens. Matter **29**, 465901 (2017).

[35] J. Klimeš, D. R. Bowler, and A. Michaelides, Chemical accuracy for the van der Waals density functional, J. Phys.: Condens. Matter **22**, 022201 (2010).

[36] R. R. D. Grande, M. G. Menezes, and R. B. Capaz, Layer breathing and shear modes in multilayer graphene: A DFT-vdW study, J. Phys.: Condens. Matter **31**, 295301 (2019).

[37] H. J. Monkhorst and J. D. Pack, Special points for Brillouin-zone integrations, Phys. Rev. B **13**, 5188 (1976).

[38] G. Trambly de Laissardière, D. Mayou, and L. Magaud, Localization of Dirac electrons in rotated graphene bilayers, Nano Lett. **10**, 804 (2010).

[39] S. Plimpton, Fast parallel algorithms for short-range molecular dynamics, J. Comput. Phys. **117**, 1 (1995).

[40] A. N. Kolmogorov and V. H. Crespi, Registry-dependent interlayer potential for graphitic systems, Phys. Rev. B **71**, 235415 (2005).

[41] W. Ouyang, D. Mandelli, M. Urbakh, and O. Hod, Nanoserpents: Graphene nanoribbon motion on two-dimensional hexagonal materials, Nano Lett. **18**, 6009 (2018).

[42] D. W. Brenner, O. A. Shenderova, J. A. Harrison, S. J. Stuart, B. Ni, and S. B. Sinnott, A second-generation reactive empirical bond order (REBO) potential energy expression for hydrocarbons, J. Phys.: Condens. Matter **14**, 783 (2002).

[43] S. J. Stuart, A. B. Tutein, and J. A. Harrison, A reactive potential for hydrocarbons with intermolecular interactions, J. Chem. Phys. **112**, 6472 (2000).

[44] L.-J. Yin, J.-B. Qiao, W.-X. Wang, W.-J. Zuo, W. Yan, R. Xu, R.-F. Dou, J.-C. Nie, and L. He, Landau quantization and Fermi velocity renormalization in twisted graphene bilayers, Phys. Rev. B **92**, 201408(R) (2015).

[45] J. M. B. Lopes dos Santos, N. M. R. Peres, and A. H. Castro Neto, Continuum model of the twisted graphene bilayer, Phys. Rev. B **86**, 155449 (2012).

[46] E. Suárez Morell, M. Pacheco, L. Chico, and L. Brey, Electronic properties of twisted trilayer graphene, Phys. Rev. B **87**, 125414 (2013).